Available online at www.sciencedirect.com
SCIENCE DIRECT®
Vision Research 44 (2004) 915–924
Vision Research
www.elsevier.com/locate/visres

Pattern detection: interactions between oriented and concentric patterns

Chien-Chung Chen [a], John M. Foley [b,*]

[a] Department of Psychology, National Taiwan University, Taipei 106, Taiwan
[b] Department of Psychology, University of California, Santa Barbara, CA 93106, USA

Received 11 June 2003; received in revised form 6 November 2003

Abstract

Target *threshold vs.* pedestal *contrast* (TvC) functions for a vertical and a concentric target were measured on a vertical, a horizontal, a plaid or a concentric Gabor pedestal. All patterns had Guassian envelopes. All except one of the TvC functions had a dipper shape, that is, the target threshold first decreased and then increased with the pedestal contrast. The TvC function for a vertical target on a horizontal pedestal was monotonically increasing. A divisive inhibition model with two orientation selective mechanisms, sensitive to vertical and horizontal, fits the data reasonably well. A significant improvement in fit is obtained by adding one or two more mechanisms. These additional mechanisms are different for different observers. Some are consistent with oblique receptive fields, some with concentric receptive fields, and some are indeterminate.

Keywords: Pattern; Detection; Threshold; Context; Masking; Contrast

1. Introduction

Most of the research on visual pattern detection and discrimination has been done with oriented patterns, frequently sinewave gratings or Gabor patches. This emphasis on oriented patterns has two roots. The first is the knowledge that most of the neurons in the primary visual cortex of animals are tuned to orientation and that different cells are tuned to different orientations (DeAngelis, Ohzawa, & Freeman, 1993; Hubel & Wiesel, 1962, 1968). There is evidence that the activations of these neurons are correlated with the visibility of the visual inputs (Tolhurst, Movshon, & Thompson, 1981). Secondly, there is psychophysical evidence that the mechanisms that mediate visual detection behavior are also orientation selective (Wilson, Levi, Maffei, Rovamo, & DeValois, 1990).

This research has led to models of pattern detection in which detection is based on the responses of an array of mechanisms with receptive fields that are oriented and tuned to spatial frequency (DeValois & DeValois, 1988; Graham, 1989; Legge & Foley, 1980; Watson, 2000; Watson & Solomon, 1997; Wilson et al., 1990; Wilson, McFarlane, & Phillips, 1983). These models describe and predict the results of many experiments done with grating and Gabor patterns. However, they have not been vigorously tested using non-oriented patterns, such as concentric patterns, as stimuli.

On the other hand, there are neurons with a concentric receptive field structure. Cells in the retina and the LGN have approximately concentric receptive fields, as do cells in the layer 4 of V1 that receive inputs from the LGN. In addition, there are cells in the ventral visual pathway in area V4 that are more sensitive to concentric patterns than to gratings (Gallant, Braun, & Van Essen, 1993; Gallant, Connor, Rakshit, Lewis, & Van Essen, 1996). Other cells are more sensitive to spirals or radial patterns. These studies do not establish that these stimuli are the best stimuli for these cells; but they are the best among the 90 sinewave grating, circular grating, spiral, and radial stimuli that were tested. Most of these cells are phase insensitive and their receptive fields cannot be mapped into excitatory and inhibitory regions. Fujita, Tanaka, Ito, and Cheng (1992) found neurons in inferior temporal cortex tuned to specific geometric patterns such as circles.

* Corresponding author. Fax: +1-805-893-4303.
E-mail address: foley@psych.ucsb.edu (J.M. Foley).

0042-6989/$ - see front matter © 2004 Elsevier Ltd. All rights reserved.
doi:10.1016/j.visres.2003.11.017

Psychophysically, there is one study that examined detection of oriented and concentric patterns. Kelly and Magnuski (1975) compared the detection of concentric patterns with sinewave gratings. They measured absolute threshold as a function of spatial frequency for sinewave gratings, zero order Bessel functions of the first kind, and circular cosine gratings. They found that at low spatial frequencies both concentric patterns had lower thresholds than sinewaves, but for frequencies above about 1 c/deg concentric patterns had thresholds that were increasingly higher than grating thresholds. A quantitative analysis of their data indicated that the threshold depends on the component of maximum magnitude in the two-dimensional Fourier transform of the stimulus patterns. These components are oriented sinewaves. This result is consistent with the hypothesis that at absolute threshold concentric pattern detection is mediated by mechanisms that have receptive fields tuned to orientation and spatial frequency. It leaves open the possibility that concentric mechanisms may be involved in the detection of concentric patterns when they are presented in the context of other patterns. This could come about if concentric mechanisms exist and oriented mechanisms are suppressed more by the context than are the concentric mechanisms.

Stromeyer and Riggs (1974) tried to test for curvature detectors in human vision using contingent aftereffects with inconclusive results. Dobbins, Zucker, and Cynader (1987) showed that the end-stopped complex cells are tuned to curvature of a light arc. This led to models in which the mechanisms responsible for curvature detection are similar to those for the detection of texture borders (Koenderink & Richards, 1988; Wilson & Richards, 1992).

Wilson, Wilkinson, and Asaad (1997) (see also Wilson & Wilkinson, 1998) measured coherence thresholds for the detection of Glass (1969) patterns in random-dot noise by varying the proportion of dot pairs oriented consistent with the dot pattern to dot pairs oriented randomly and determining the proportion that corresponded to 75% correct. They found that concentric Glass patterns had substantially lower thresholds than radial, hyperbolic, or parallel patterns. They also showed that the degree of spatial summation is nearly perfect for concentric patterns, suggesting that a single concentric mechanism is responsible for the detection. They found less summation for radial glass patterns and least for parallel glass patterns. They proposed a four-stage model, in which the Glass pattern detectors essentially linearly sum the outputs of curvature detectors (Wilson & Richards, 1992), to account for their results. Recent results, however, indicate that the greater sensitivity to concentric Glass patterns is not a general finding and may be a consequence of the use of a circular window in the Wilson et al. experiments (Dakin & Bex, 2002).

Other recent research on spatial vision suggests that concentric mechanisms have an important role in the discrimination of patterns that contain two or more sinewave components. For instance, Thomas and Olzak (1996) (also see Olzak & Thomas, 1999) proposed a two-stage model for pattern discrimination. The first stage of their model consists of a set of oriented linear filters tuned to different orientations and spatial frequencies. Each mechanism in the second stage pools information from the first stage filters. One type of second stage mechanism pools information from the first stage filters of all orientation preferences, but tuned to the same spatial frequency. In the Fourier domain, the sensitivity profile of these second stage mechanisms has an annulus, or "doughnut", shape. Thus, in the space domain, the sensitivity profile of such a mechanism has a concentric shape. However, none of these papers propose that concentric mechanisms are involved in contrast pattern detection.

In principle, the responses of cells at different levels in the visual system could provide the basis for pattern detection when patterns are presented in the context of other patterns. Current models of pattern detection require that responses be summed nonlinearly across all the mechanisms that contribute to detection. It is possible that the behavioral response in a detection task could be determined by neural responses occurring at any of several levels of the system and therefore be determined by cells tuned both to oriented and concentric patterns. Experiments in which target patterns are detected in various contexts (sometimes referred to as masking experiments) have been important in testing theories of pattern detection and revealing underlying mechanisms. How target threshold changes or fails to change with the context provides information about how the context influences the response of the mechanism. More specifically, the *target threshold vs. pedestal contrast function* (TvC function) has been particularly useful (Foley, 1994; Legge & Foley, 1980).

Our goal in this study was to measure TvC functions when either the target or the context or both were concentric patterns, to determine whether the results could be described by a model of pattern vision that has worked well with other patterns (Foley, 1994; Foley & Chen, 1999), and, if so, to use the model to estimate the sensitivity of the detecting mechanisms.

We measured TvC functions for the detection of a vertical Gabor patch and a concentric Gabor patch in the presence of a vertical Gabor, a horizontal Gabor, a plaid Gabor, and a concentric Gabor (concentric cosine with a Gaussian envelope).

2. Method

2.1. Apparatus

The stimuli were generated using a computer graphics system that consisted of a PC type computer, a Truevision ATVISTA graphics board with 2 MB video memory, a contrast mixer and attenuator circuit, and two video monitors (Sony, model CPD-1304). Truevision Stage graphics software was used for image generation and control. The pedestal was generated on one monitor and the target on the other, and they were combined by a beam splitter. The resolution of the monitor was 512×400 pixels. Viewed at a distance of 162 cm, the width of each pixel is approximately 1 min. The intensity of an image was specified by an 8-bit indexed lookup table. The frame rate was 60 Hz. The methods of contrast control described by Watson, Nielsen, Poirson, and Fitzhugh (1986) were adapted to our system and experimental paradigm. The pedestal and the target contrasts were controlled independently by lookup tables and could be further attenuated by an analog circuit to produce low contrasts without loss of waveform definition. The lookup tables had the dual role of controlling contrast and correcting for the nonlinear relation between voltage and screen intensity.

2.2. Stimuli

We measured the threshold of a target pattern superimposed on another pattern (pedestal). We used four types of patterns for both targets and pedestals: vertical Gabor, horizontal Gabor, plaid, and concentric Gabor. These stimuli and their Fourier amplitude spectra are illustrated in Fig. 1. The light intensity of any point (x, y) from the center of a vertical Gabor was defined by the equation:

$$L(x,y) = L(1 + C\cos(2\pi fx)\exp(-x^2/\sigma^2)\exp(-y^2/\sigma^2)), \quad (1)$$

where L was the background luminance, C is the contrast of the pattern, f was the spatial frequency, and σ was the $1/e$ space constant. In our experiment, the spatial frequency was 2 cycles per degree and σ was 0.5 degree. The horizontal Gabor was defined in a similar way by swapping x and y in Eq. (1). The concentric pattern was defined by the equation:

$$L(r) = L(1 + C\cos(2\pi fr)\exp(-r^2/\sigma^2)), \quad (2)$$

where $r = (x^2 + y^2)^{0.5}$ is the radial distance. For the horizontal, vertical, and concentric Gabors contrast is defined as the Michelson contrast of the underlying sinewave. The plaid was the sum of a vertical and a horizontal Gabor pattern. Its contrast was defined as the sum of the two component contrasts.

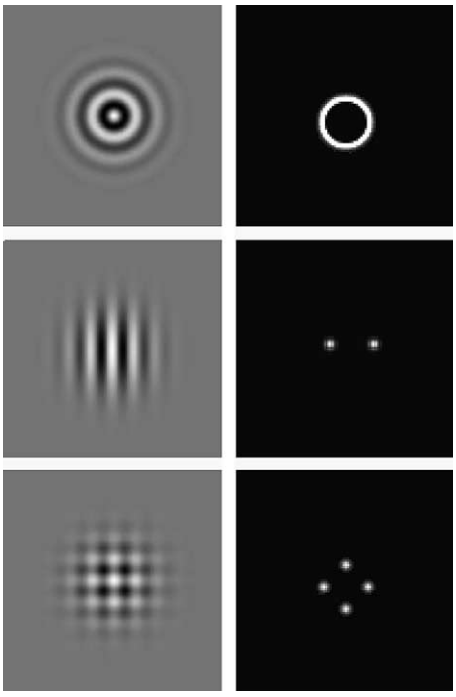

Fig. 1. Left: the three types of pattern used in this experiment. Top: concentric Gabor pattern. Middle: vertical Gabor pattern; the horizontal Gabor was identical except for orientation. Bottom: plaid pattern; the sum of the vertical and horizontal Gabor patterns, each at half the contrast of the plaid. Right: the amplitude of the two-dimensional Fourier transform of each stimulus on the left.

2.3. Procedure

The target contrast threshold was measured with a temporal two-alternative forced-choice paradigm. The pedestal was presented in both temporal intervals. The target was randomly presented in one of the two intervals with a probability of 0.5. The target and the pedestal were presented concurrently in the target interval. They had a duration of 33 ms (two frames). The two intervals were separated by 660 ms. An auditory feedback was given to the observer after each trial. The QUEST procedure (Watson & Pelli, 1983) was used to adjust the contrast so as to determine the target threshold at the 0.91 probability correct level. The QUEST sequence was terminated after 40 trials, or 50 trials if there were no errors on the last 20 trials.

Two of the observers made phenomenological reports of the appearance of the target at threshold with and without the masks over the range of mask contrasts.

2.4. Experimental Design

There were eight conditions corresponding to the two targets each paired with the four pedestals. In each condition we measured the target contrast threshold for 10 contrasts of the pedestal and no pedestal (absolute threshold). In a typical session a single condition was

used and the 10 pedestal contrasts and no pedestal condition were presented in random order. Each of the eight conditions was presented four times over the course of the experiment, except for CCC for whom each condition was presented three times. In a few conditions where variance was high additional measurements were made. An outlier test was used and 44/1584 measurements (2.8%) were excluded from analysis on the basis of this test.

There were five observers. CCC and JMF are the authors and the other three were naive with respect to the purpose of the experiment. Observer WSC completed only 6 or the 8 conditions. All had visual acuity of 20/20 or better, with or without correction, and no known visual problems.

3. Results

Qualitatively, there is good agreement among the five observers. Except for the one case in which target and pedestal are orthogonal, all the TvC functions have a dipper shape, that is, as pedestal contrast increases the target threshold first decreases and then increases. Because the functions for individual observers are not completely smooth, we computed the average thresholds across the five observers. These mean thresholds are shown in Fig. 2, The mean standard error of these measurements is 0.83 dB with a slight tendency for standard error to increase with pedestal contrast. The smooth curves through the data correspond to a model that will be described below.

When the target is a vertical Gabor pattern, the vertical Gabor pedestal facilitates and masks more than the other pedestals. The horizontal pedestal does not facilitate at all and masks weakly, as has been shown previously (Foley, 1994). The plaid pedestal produces a TvC function that has a form very similar to that for the vertical pedestal, but shifted to the right by 5–6 dB. This shift coincides approximately with the difference in contrast between vertical pedestal and the vertical component in the plaid pedestal. The concentric pedestal facilitates less than the vertical or plaid pedestals and produces a magnitude of masking which is between that produced by the vertical pedestal and that produced by the plaid.

When the target is concentric, the concentric pedestal facilitates and masks more than the other pedestals. The horizontal and vertical pedestals produce similar TvC functions, with the function for the horizontal pedestal being shifted about 2 dB to the right. The functions for the horizontal and vertical pedestals have a somewhat different form than the others; rising rapidly at first and then more slowly. The plaid pedestal facilitates more than the vertical or horizontal pedestals, and masking increases almost as rapidly for the plaid as for the concentric pedestal. The absolute threshold for the vertical target is about 2 dB (or 26%) lower than the threshold for the concentric target. This difference is slightly smaller than that reported by Kelly and Magnuski (1975).

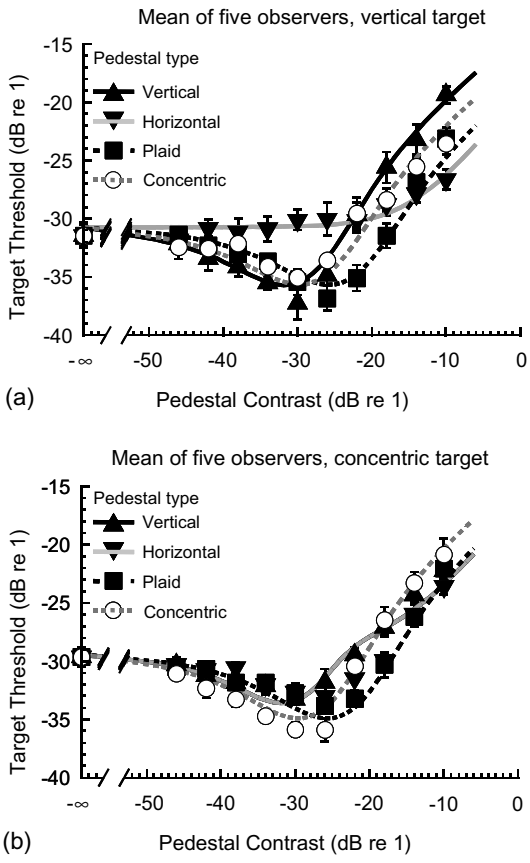

Fig. 2. Threshold vs Pedestal Contrast (TvC) functions for the mean thresholds over the five observers: (a) vertical target and (b) concentric target. Smooth curves are best fit of a two oriented mechanism model (models 2–6) to the data. Here the predictions for the vertical and horizontal pedestals are the same.

4. Discussion

4.1. Basic model

We addressed two theoretical questions with respect to these results. First, are the results consistent with a version of the nonlinear excitation/divisive inhibition model (Chen, Foley, & Brainard, 2000; Foley, 1994; Foley & Chen, 1999); second, if so, how many mechanisms are required to account for these results and what are their sensitivities? The class of models that we fitted is illustrated in Fig. 3.

In this class of models pattern detection is mediated by pattern vision mechanisms. These mechanisms are sensitive to the contrast of patterns. The excitation produced by a pattern, i, in a mechanism, j, is the

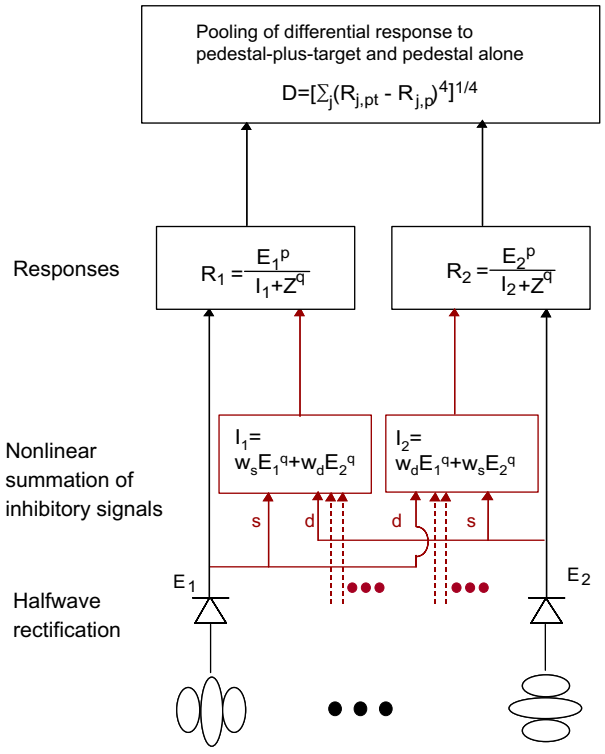

Fig. 3. Schematic illustration of the nonlinear excitation/divisive inhibition model. In this illustration, we only show two mechanisms. However, it is not difficult to extend it to multiple mechanisms, and most of the models that we considered have three or four mechanisms.

product of the contrast of the pattern C_i the sensitivity of the mechanism to that pattern, s_{ij}:

$$E'_{ij} = s_{ij}C_i. \tag{3}$$

Sensitivities and excitations may be positive or negative. The sum of the excitations produced by each pattern is given by:

$$E'_j = \sum_i E'_{ij}. \tag{4}$$

This sum is halfwave rectified to give the net excitation of the mechanism:

$$E_j = \max\left(0, E'_j\right). \tag{5}$$

Each mechanism produces divisive inhibition in itself and in all the other mechanisms. The inhibitory signal from mechanism k to mechanism j is the product of an inhibitory weight, w_{jk}, and the net excitation raised to the power q:

$$I_{jk} = w_{jk}E_k^q, \tag{6}$$

where the inhibitory weights are constrained to be positive.

The total inhibition on mechanism j is:

$$I_j = \sum_{j,k} I_{jk}. \tag{7}$$

The response of mechanism j is given by the nonlinear equation:

$$R_j = E_j^p/\left(I_j + Z_j^q\right). \tag{8}$$

The threshold depends on the value of a detection variable that is a nonlinear sum over all the mechanisms of the difference between the response to the pedestal plus the target and the response to target alone:

$$d = \left[\sum_j \left(R_{j,p+t} - R_{j,p}\right)^4\right]^{1/4}. \tag{9}$$

A target is at threshold when $d = 1$.

The version of the model that we have used here is constrained in the following ways: The parameters p, q, and Z are the same for all mechanisms. There are only two inhibitory weights, one for self-inhibition, w_s, and one for inhibition from different mechanisms, w_d, which are also the same for all mechanisms. We explored models that allow more flexibility in the inhibitory weights and we found that they improve very little on the goodness of fit of the best models reported here.

The models that we considered varied in the number of mechanisms assumed and in the constraints on the excitatory sensitivities of these mechanisms. We started with a simple two-mechanism model and we proceeded by relaxing constraints and adding mechanisms until we no longer obtained a statistically significant improvement in goodness of fit. The models are identified by two numbers separated by a hyphen. The first number is the number of mechanisms and the second number is the number of free parameters. Each model had the five free parameters: p, q, Z, and the two inhibitory weights. The other free parameters were excitatory sensitivities of the mechanisms to the stimulus patterns.

We used four patterns, which we designate by v (vertical), h (horizontal), c (concentric), and p (plaid). We considered models that have a mechanism sensitive to vertical, but not horizontal patterns (V-mechanism), a mechanism sensitive to horizontal, but not vertical patterns, (H mechanism). Some of the models have a mechanism sensitive to concentric, but not to vertical or horizontal patterns (O mechanism). Some have a mechanism (A mechanism) that has non-zero sensitivity to all four patterns.

The data were fitted by a Powell's algorithm (Press, Teukolsky, Vetterling, & Flannery, 1986) that seeks the parameter values that minimize the sum of the squared differences between the measured and predicted thresholds (SSE). Since there are local minima in the SSE space, we made 50 fits, each starting from a different initial set of parameter values to determine the best fit.

The simple two-mechanism models 2–6 (see Table 1), has a mechanism sensitive to the vertical Gabor and not the horizontal (V-mechanism) and a mechanism sensitive to the horizontal Gabor and not the vertical

Table 1
Summary of model fits to the simplest model and the two best models

Characteristics of the data sets

							Data set			
						CCC	EAH	JMF	MAB	WSC	ALL
Number of TvC functions						8	8	8	8	6	8
Number of data points						86	88	88	88	66	88
Mean standard error						0.77	0.66	0.70	0.79	0.65	0.83
RMSE best						1.415	0.909	1.22	1.184	0.999	0.70
RMSE best/mean SE						1.845	1.385	1.752	1.505	1.534	0.846
Model2–6											
	Mechanisms				SSE		213.61	109.92	211.08	178.54	85.86	70.94
Stimuli	V	H			RMSE		1.58	1.12	1.55	1.42	1.14	0.90
v	s1	0			Free parameters		6	6	6	6	6	6.00
h	0	s1										
c	s2	s2				s2	91.49	71.21	85.72	73.25	81.36	78.78
p	.5xs1	.5xs1				ws	1.19	0.42	0.48	0.28	0.51	0.55
						wd	0.0078	0.0354	0.02	0.04	0.0315	0.02
						Z	3.86	2.41	3.02	2.95	2.12	2.93
						p	3.58	2.07	2.46	2.24	2	2.51
						q	3	1.71	2.03	1.98	1.63	2.09
Model 3–9												
					SSE		189.35	72.74	130.62	142.02	73.82	52.42
	V	H	A		RMSE		1.484	0.909	1.22	1.27	1.058	0.77
v	s1	0	s4		Free Parameters		9	9	9	9	9	9.00
h	0	s2	s4									
c	fxs1	fxs2	s3			s2	106.75	72.44	78.01	80.26	89.02	85.91
p	.5xs1	.5xs2	s4			s3	105.65	82.1	82.08	80.29	24.43	61.12
						s4	-9.86	-7.46	58.01	-5.03	51.32	40.40
						f	0.83	0.75	0.35	0.76	0.88	0.80
						ws	1.03	0.44	0.2	0.31	0.57	0.55
The best fit to each data						wd	0.0087	0.0357	0.44	0.04	0.0164	0.03
set is highlighted with gray.						Z	2.43	2.48	2.68	3.01	2.22	2.83
						p	3.14	2.22	2.52	2.44	2.25	2.49
						q	2.72	1.85	2.15	2.16	1.87	2.07
Model 4–11												
					SSE		172.24	70.32	121.89	123.3	65.55	43.45
	V	H	O	A	RMSE		1.415	0.894	1.177	1.184	0.999	0.70
v	s1	0	0	s4	Free Parameters		11	11	11	11	11	11.00
h	0	s2	0	s5								
c	f*s1	f*s2	s3	s6		s2	111.83	81.76	92.15	84.88	88.26	86.02
p	.5*s1	.5*s2	0	.5xs4+.5xs5		s3	67.24	51.01	85.18	77.98	91.36	79.52
						s4	-15.4	91.94	58.41	-231.34	72.58	50.63
						s5	-5.49	-119.12	48.97	93.65	27.16	37.64
						s6	107.15	-0.46	71.96	-95.61	2.13	66.24
						f	0.79	0.78	-0.0539	0.74	0.82	0.77
						ws	1.09	0.42	0.58	0.34	0.62	0.58
						wd	0.0041	0.0277	0.0154	0.0490	0.0220	0.0314
						Z	3.87	2.49	2.74	3.01	2.27	2.87
						p	3.76	2.17	3.05	2.55	2.4	2.60
						q	3.21	1.82	2.57	2.24	2.01	2.18

Best model		**47**	**35**	**35**	**47**	**47**	**47**
Mechanisms		**H**	**V**	**V**	**V**	**V**	**V**
		V	**O**	**C or O**	**H**	**O**	**H**
		O	**H**	**H**	**O**	**H**	**O**
		O		**?**		**?**	**C or 0**

Mechanisms are listed in the order of their sensitivity to their best stimulus from greatest to least.

The columns on the right side correspond to the six data sets, one for each observer and one for the mean across observer. The first section describes some characteristics of the data sets. Each of the following sections describes the fit of one of the three models to the six data sets. On the left is a table that shows the excitatory sensitivities of each mechanism in the model to each of the four stimulus patterns and the constraints on these sensitivities. The columns on the right summarize the best fit of this model to each of the six data sets. This summary includes the sum of squared error of the fit, the root mean squared error, the number of free parameters and the values of these parameters for the best fit. The best fit to each data set is highlighted in gray. The table at the bottom shows the mechanism types in the best model.

(H-mechanism). They have equal sensitivity to the vertical and horizontal patterns, respectively, and both are equally sensitive to the concentric pattern. They also have equal sensitivity to the plaid, which is assumed to be half their sensitivity to either the vertical or the horizontal pattern.

This heavily constrained model fits the data reasonably well. Table 1 shows the parameter values and the root mean squared error (RMSE) for this model. The fits of the model to the mean data of observers are shown in Fig. 2 as smooth curves. The RMSE is only slightly larger than the standard error. There is systematic over-estimation of the threshold for the concentric target on the concentric pedestal and under-prediction on the plaid pedestal. The model was also fitted to the individual data sets. These fits were not as good. The RMSEs for individual observers are about two times the standard error of the measurements.

4.2. Other possible models

We proceeded to fit 13 other models that differed in the number of mechanisms and the constraints placed on their sensitivities. These models seemed to us to be plausible alternatives; they do not exhaust the set of possible 3 and 4 mechanisms models. All of the mechanisms were of the four types described above, V, H, O, and A. Most of the models formed a nested set and we found the "best" model for each data set, which we defined as the model whose best fit was not improved to a statistically significant extent ($P > 0.05$) by adding additional free parameters (Table 2). We did a test for improvement in fit to determine in which cases the improvement in fit is statistically significant (Khuri & Cornell, 1987). A summary of the best fits to two of these models is given in Table 1. The best model for each of the six data sets is highlighted with a gray background. Models 3–9 (a three-mechanism model with nine free parameters) was best for EAH and JMF; models 4–11 (a four mechanism model with 11 free parameters) was best for CCC, MAB, WSC and ALL (average across observers). The RMSE of these best fits

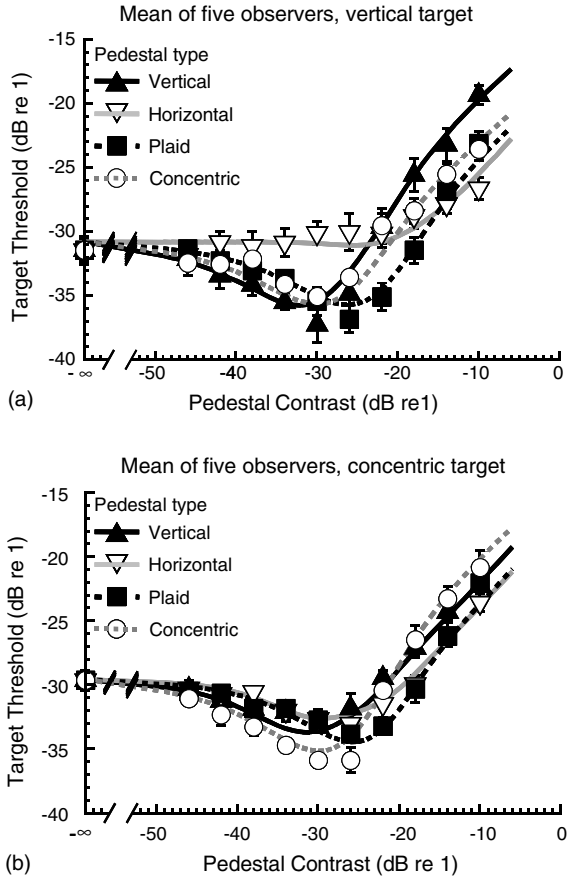

Fig. 4. Threshold vs Pedestal Contrast (TvC) functions for the mean thresholds over the five observers: (a) vertical target and (b) concentric target. Smooth curves correspond to the predictions of the best fitting model (models 4–11).

Table 2
Tests of statistical significance of improvement in fit for nested models

Models 3–9 vs 2–6						
F	**3.288**	**13.460**	**16.221**	**6.772**	**3.099**	**9.304**
df num	3	3	3	3	3	3
df den	77	79	79	79	57	79
p	**0.0251**	**0.0000**	**0.0000**	**0.0004**	**0.0314**	**0.0000**
Models 4–11 vs 2–6						
F	**3.603**	**8.672**	**11.269**	**6.899**	**3.408**	**9.743**
df num	5	5	5	5	5	5
df den	75	77	77	77	55	77
p	**0.0056**	**0.0000**	**0.0000**	**0.0000**	**0.0094**	**0.0000**
Models 4–11 vs 3–9						
F	**3.725**	**1.325**	**2.757**	**5.845**	**3.469**	**7.948**
df num	2	2	2	2	2	2
df den	75	77	77	55	55	77
p	**0.0287**	0.2718	0.0697	**0.005**	**0.0381**	**0.0007**

$F = ((\text{SSEred} - \text{SSEfull})/(\text{par\_full} - \text{par\_red}))/(\text{SSEfull})/(\text{data\_pts} - \text{par\_full})$, where the number of degrees of freedom for the numerator equals the difference in the number of free parameters. The number of degrees of freedom for the denominator equals the number of degrees of freedom for the full model. This corresponds to the number of data points minus the number of free parameters. Values of F that are significant at the 0.05 level are in bold print.

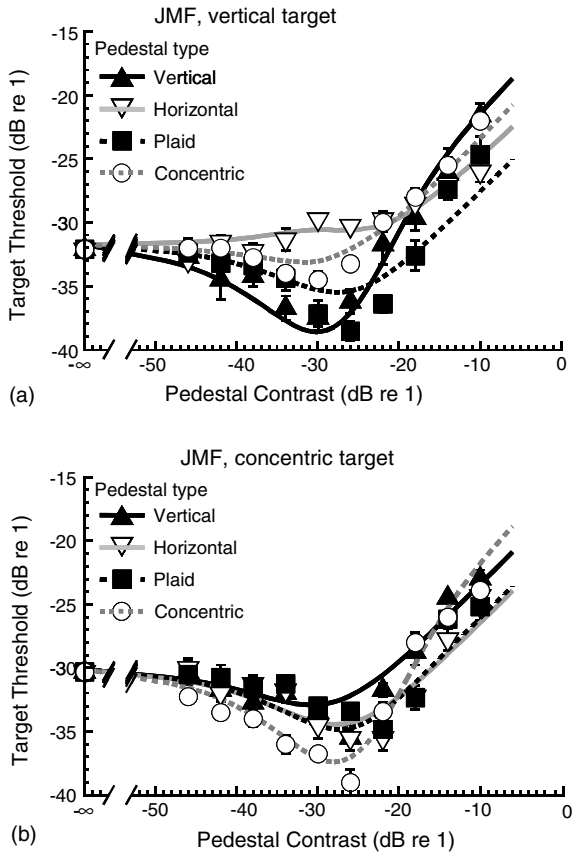

Fig. 5. Threshold vs Pedestal Contrast (TvC) functions for the mean thresholds of Observer JMF: (a) vertical target and (b) concentric target. Smooth curves correspond to the predictions of the best fitting model (models 3–9).

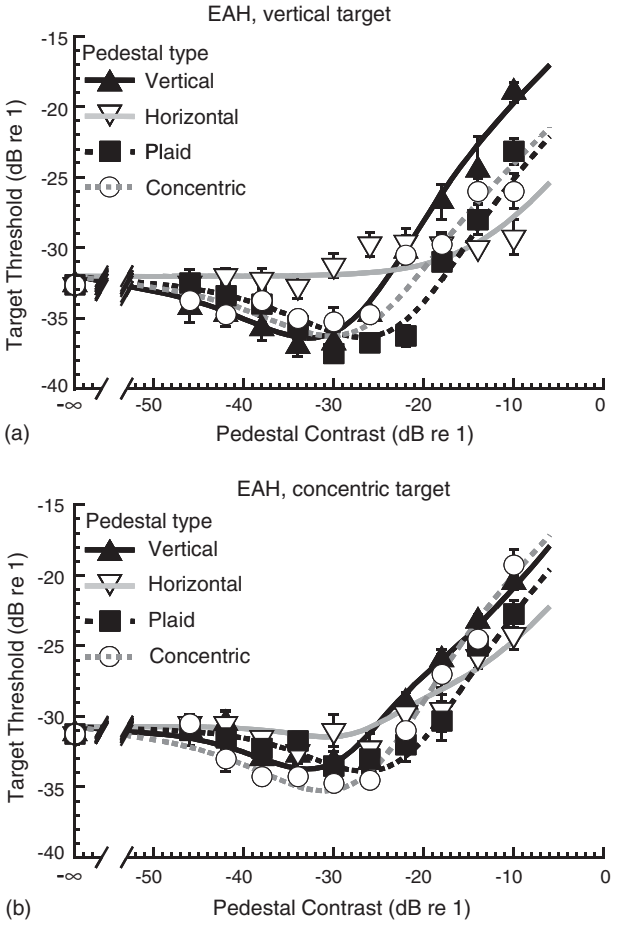

Fig. 6. Threshold vs Pedestal Contrast (TvC) functions for the mean thresholds of Observer EAH: (a) vertical target and (b) concentric target. Smooth curves correspond to the predictions of the best fitting model (models 3–9).

averages 1.48 times the standard error. Fig. 4 shows the best fit to the average across observers. Figs. 5 and 6 show the best fits for two individual observers.

The excitatory sensitivity parameters (Table 1) indicate which mechanisms were involved in the detection of each pattern. In the two-mechanism model the vertical target was detected by the V mechanism, the horizontal pattern by the H mechanism, and the plaid and concentric patterns by both mechanisms. In the other two models, the V and H mechanisms are sensitive to these same patterns, the O mechanism is sensitive only to the concentric pattern, and the A mechanism is sensitive to all four patterns.

The difference between these two best models is that models 4–11 has an O mechanism that is sensitive to concentric, but not sensitive to vertical or horizontal patterns. An oriented mechanism sensitive to an oblique orientation would have these properties (e.g., a mechanism tuned to 45 deg with narrow tuning function). There is both psychophysical and physiological evidence for the existence of such mechanisms. What is most interesting in these best models is the nature of the A mechanism. For JMF, WSC and ALL this mechanism has positive sensitivity to vertical, horizontal, and concentric patterns. For the other three observers this mechanism has a negative sensitivity to one or two of these stimuli.

In order to get a better understanding of the implications of these model fits, for each of the mechanisms in the best models, we computed a receptive field whose sensitivities to the four patterns correspond most closely to those of the model mechanism. These receptive fields were constrained to have Gabor spatial sensitivity profiles with a center spatial frequency of 2 c/deg in cosine phase with and centered on the target patterns or Gaussian windowed concentric cosine receptive fields of the same frequency. The orientation, the width and height space constants, and the maximum sensitivity of the Gabor receptive fields were varied to find the best match to the sensitivities of the model mechanisms; only the radial space constant and the maximum sensitivity of the concentric receptive fields were varied. The V and H mechanisms correspond to Gabor receptive fields that have space constants of about 0.5 deg in both width and

height, but are tilted away from the vertical and horizontal by about 20 deg. This tilt is a consequence of the ratio of their sensitivity to the vertical (or horizontal) pattern to their sensitivity to the concentric pattern.

The receptive fields corresponding to the A mechanisms are harder to characterize. For three observers they have positive sensitivities to all four patterns and so they must be very broadly tuned to orientation. For JMF and ALL either a concentric receptive field or a small oriented Gabor receptive field can have a similar pattern of sensitivities. For ALL the concentric field is not isotropic. All these receptive fields are small with envelope standard deviations of 0.12 deg or less. For WSC neither type of receptive field fits the sensitivities well.

For CCC and EAH the negative sensitivities of the A mechanism are small and setting them to 0 has little effect on goodness of fit, which means that this could be a second oblique mechanism. The A mechanism sensitivities for MAB do not correspond to any Gabor receptive field. So for this observer, as for WSC, we did not find either type of receptive field with a closely corresponding set of sensitivities.

In conclusion, a three or four mechanism model fits each of the data sets well with RMSEs less than 1.5 times the standard error of the measurement. The sensitivities of most of the model mechanisms correspond to those of oriented Gabor receptive fields of plausible sizes. Two of the A mechanisms could have small oriented receptive fields or concentric receptive fields. For two others, neither of these receptive field types has a corresponding pattern of sensitivities.

Acknowledgements

This research was supported by NIH grant EY12734.

References

Chen, C. C., Foley, J. M., & Brainard, D. H. (2000). Detection of chromoluminance patterns on chromoluminance pedestals II: Model. *Vision Research, 40*, 789–803.

Dakin, S. C., & Bex, P. J. (2002). Summation of concentric orientation structure: Seeing the Glass or the window? *Vision Research, 42*, 2013–2020.

DeAngelis, G. C., Ohzawa, I., & Freeman, R. D. (1993). Spatiotemporal organization of simple-cell receptive fields in the cat's striate cortex. II. Linearity of temporal and spatial summation. *Journal of Neurophysiolgy, 69*, 1118–1135.

DeValois, R. L., & DeValois, K. K. (1988). *Spatial vision*. New York: Oxford University Press.

Dobbins, A., Zucker, S. W., & Cynader, M. S. (1987). Endstopped neurons in the visual cortex as a substrate for calculating curvature. *Nature, 329*, 438–441.

Foley, J. M. (1994). Human luminance pattern-vision mechanisms: Masking experiments require a new model. *Journal of the Optical Society of America A, 11*, 1710–1719.

Foley, J. M., & Chen, C. C. (1999). Pattern detection in the presence of maskers that differ in spatial phase and temporal offset: Threshold measurements and a model. *Vision Research, 39*, 3855–3872.

Fujita, I., Tanaka, K., Ito, M., & Cheng, K. (1992). Columns for visual features of objects in monkey inferotemporal cortex. *Nature, 360*, 343–346.

Gallant, J. L., Braun, J., & Van Essen, D. C. (1993). Selectivity for polar, hyperbolic, and cartesian gratings in Macaque visual-cortex. *Science, 259*, 100–103.

Gallant, J. L., Connor, C. E., Rakshit, S., Lewis, J. W., & Van Essen, D. C. (1996). Neural responses to polar, hyperbolic, and Cartesian gratings in area V4 of the macaque monkey. *Journal of Neurophysiology, 76*, 2718–2739.

Glass, L. (1969). Moire effect from random dots. *Nature, 223*, 578–580.

Graham, N. V. S. (1989). *Visual pattern analyzers*. New York: Oxford University Press.

Hubel, D. H., & Wiesel, T. N. (1962). Receptive fields, binocular interaction and functional architecture in the cat's visual cortex. *Journal of Physiology, 160*, 106–154.

Hubel, D. H., & Wiesel, T. N. (1968). Receptive fields and functional architecture of monkey striate cortex. *Journal of Physiology, 195*, 215–243.

Kelly, D. H., & Magnuski, H. S. (1975). Pattern detection and the two-dimensional fourier transform: Circular targets. *Vision Research, 15*, 911–915.

Khuri, A. A., & Cornell, J. A. (1987). *Response surfaces: Designs and analysis*. New York: Dekker.

Koenderink, J. J., & Richards, W. (1988). Two-dimensional curvature operators. *Journal of the Optical Society of America A, 5*, 1136–1141.

Legge, G. E., & Foley, J. M. (1980). Contrast masking in human vision. *Journal of the Optical Society of America, 70*, 1458–1471.

Olzak, L. A., & Thomas, J. P. (1999). Neural recoding in human pattern vision: Model and mechanisms. *Vision Research, 39*, 231–256.

Press, W. H., Teukolsky, S. A., Vetterling, W. T., & Flannery, B. P. (1986). *Numerical recipes*. Cambridge: Cambridge University Press.

Stromeyer, C. F., & Riggs, L. A. (1974). Curvature detectors in human vision? *Science, 184*, 1199–1200.

Thomas, J. P., & Olzak, L. A. (1996). Uncertainty experiments support the roles of second-order mechanisms in spatial frequency and orientation discriminations. *Journal of the Optical Society of America A, 13*, 689–696.

Tolhurst, D. J., Movshon, J. A., & Thompson, I. D. (1981). The dependence of response amplitude and variance of cat visual cortical neurones on stimulus contrast. *Experimental Brain Research, 41*, 414–419.

Watson, A. B. (2000). Visual detection of spatial contrast patterns: Evaluation of five simple models. *Optics Express, 6*, 12–33.

Watson, A. B., Nielsen, K. R., Poirson, A., & Fitzhugh, A. (1986). Use of a raster framebuffer in vision research. *Behavior Research Methods, Instruments and Computers, 18*, 587–594.

Watson, A. B., & Pelli, D. G. (1983). Quest: A bayesian adaptive psychometric method. *Perception and Psychophysics, 33*, 113–120.

Watson, A. B., & Solomon, J. A. (1997). Model of visual contrast gain control and pattern masking. *Journal of the Optical Society of America, 14*, 2379–2391.

Wilson, H. R., Levi, D., Maffei, L., Rovamo, J., & DeValois, R. (1990). The perception of form: Retina to striate cortex. In L. Spillmann & J. S. Werner (Eds.), *Visual perception: The neurological foundations*. San Diego: Academic Press.

Wilson, H. R., McFarlane, D. K., & Phillips, G. C. (1983). Spatial frequency tuning of orientation selective units estimated by oblique masking. *Vision Research, 23*, 873–882.

Wilson, H. R., & Richards, W. (1992). Curvature and separation discrimination at texture boundaries. *Journal of the Optical Society of America A, 9*, 1653–1662.

Wilson, H. R., & Wilkinson, F. (1998). Detection of global structure in Glass patterns: Implications for form vision. *Vision Research, 38*, 2933–2947.

Wilson, H. R., Wilkinson, F., & Asaad, W. (1997). Rapid communication: Concentric orientation summation in human form vision. *Vision Research, 37*, 2325–2330.